Transverse momentum fluctuations in nuclear collisions at 158*A* GeV

T. Anticic,[21] B. Baatar,[9] D. Barna,[4] J. Bartke,[7] M. Behler,[14] L. Betev,[10] H. Bialkowska,[19] A. Billmeier,[10] C. Blume,[8] B. Boimska,[19] M. Botje,[1] J. Bracinik,[3] R. Bramm,[10] R. Brun,[11] P. Bunčić,[10,11] V. Cerny,[3] P. Christakoglou,[2] O. Chvala,[16] J. G. Cramer,[17] P. Csató,[4] N. Darmenov,[18] A. Dimitrov,[18] P. Dinkelaker,[10] V. Eckardt,[15] P. Filip,[15] D. Flierl,[10] Z. Fodor,[4] P. Foka,[8] P. Freund,[15] V. Friese,[8] J. Gál,[4] M. Gaździcki,[10] G. Georgopoulos,[2] E. Gładysz,[7] K. Grebieszkow,[20] S. Hegyi,[4] C. Höhne,[14] K. Kadija,[21] A. Karev,[15] V. I. Kolesnikov,[9] T. Kollegger,[10] R. Korus,[13] M. Kowalski,[7] I. Kraus,[8] M. Kreps,[3] M. van Leeuwen,[1] P. Lévai,[4] L. Litov,[18] M. Makariev,[18] A. I. Malakhov,[9] C. Markert,[8] M. Mateev,[18] B. W. Mayes,[12] G. L. Melkumov,[9] C. Meurer,[10] A. Mischke,[8] M. Mitrovski,[10] J. Molnár,[4] St. Mrówczyński,[13] G. Pálla,[4] A. D. Panagiotou,[2] D. Panayotov,[18] A. Petridis,[2] M. Pikna,[3] L. Pinsky,[12] F. Pühlhofer,[14] J. G. Reid,[17] R. Renfordt,[10] W. Retyk,[20] C. Roland,[6] G. Roland,[6] M. Rybczyński,[13] A. Rybicki,[7,11] A. Sandoval,[8] H. Sann,[8] N. Schmitz,[15] P. Seyboth,[15] F. Siklér,[4] B. Sitar,[3] E. Skrzypczak,[20] G. Stefanek,[13] R. Stock,[10] H. Ströbele,[10] T. Susa,[21] I. Szentpétery,[4] J. Sziklai,[4] T. A. Trainor,[17] D. Varga,[4] M. Vassiliou,[2] G. I. Veres,[4] G. Vesztergombi,[4] D. Vranić,[8] A. Wetzler,[10] Z. Włodarczyk,[13] I. K. Yoo,[5] J. Zaranek,[10] and J. Zimányi[4]

[1]*NIKHEF, Amsterdam, Netherlands*
[2]*Department of Physics, University of Athens, Athens, Greece*
[3]*Comenius University, Bratislava, Slovakia*
[4]*KFKI Research Institute for Particle and Nuclear Physics, Budapest, Hungary*
[5]*Department of Physics, Pusan National University, Busan, Republic of Korea*
[6]*MIT, Cambridge, Massachusetts, USA*
[7]*Institute of Nuclear Physics, Cracow, Poland*
[8]*Gesellschaft für Schwerionenforschung (GSI), Darmstadt, Germany*
[9]*Joint Institute for Nuclear Research, Dubna, Russia*
[10]*Fachbereich Physik der Universität, Frankfurt, Germany*
[11]*CERN, Geneva, Switzerland*
[12]*University of Houston, Houston, Texas, USA*
[13]*Institute of Physics Świetokrzyska Academy, Kielce, Poland*
[14]*Fachbereich Physik der Universität, Marburg, Germany*
[15]*Max-Planck-Institut für Physik, Munich, Germany*
[16]*Institute of Particle and Nuclear Physics, Charles University, Prague, Czech Republic*
[17]*Nuclear Physics Laboratory, University of Washington, Seattle, Washington, USA*
[18]*Atomic Physics Department, Sofia University St. Kliment Ohridski, Sofia, Bulgaria*
[19]*Institute for Nuclear Studies, Warsaw, Poland*
[20]*Institute for Experimental Physics, University of Warsaw, Warsaw, Poland*
[21]*Rudjer Boskovic Institute, Zagreb, Croatia*

(Received 17 November 2004; published 10 September 2004)

Results are presented on event-by-event fluctuations in transverse momentum of charged particles, produced at forward rapidities in p+p, C+C, Si+Si, and Pb+Pb collisions at 158 *A*GeV. Three different characteristics are discussed: the average transverse momentum of the event, the Φ_{p_T} fluctuation measure, and two-particle transverse momentum correlations. In the kinematic region explored, the dynamical fluctuations are found to be small. However, a significant system size dependence of Φ_{p_T} is observed, with the largest value measured in peripheral Pb+Pb interactions. The data are compared with predictions of several models.

DOI: 10.1103/PhysRevC.70.034902 PACS number(s): 25.75.Gz

I. INTRODUCTION

Nucleus-nucleus (A+A) collisions at relativistic energies have been intensely studied over the last two decades. The main goal of these efforts is to understand the properties of strongly interacting matter under extreme conditions of high energy and baryon densities when the creation of the quark-gluon plasma (QGP) is expected [1]. Experimental results obtained in a broad range of collision energies indicate that an extended zone of strongly interacting dense matter indeed occurs in the collision process. Various collision characteristics and their collision energy dependence suggest [2,3] that a transient state of deconfined matter may be created at collision energies as low as 40 *A*GeV.

QGP formation is expected to occur at the early collision stage when the system is sufficiently hot and dense. In the course of further evolution, the system dilutes and cools down, hadronizes, and finally decays into free hadrons. Therefore, the final state hadrons carry only indirect information about the early stage of the collision. Thus, firm conclusions about the creation of deconfined matter require studying a variety of collision characteristics.

As fluctuations are sensitive to the dynamics of the system, in particular at the phase transition, the analysis of

event-by-event fluctuations has been proposed as an important tool in the study of A+A collisions [4]. Large acceptance detectors, which allow the observation of a significant fraction of the final state particles, have made this suggestion truly attractive [5]. First pioneering studies were carried out by the NA49 collaboration on the fluctuations of the average transverse momentum [6] and the K/π ratio [7] in central Pb+Pb collisions at the CERN super proton synchrotron (SPS). Transverse momentum fluctuations were further studied in several experiments at the CERN SPS [8,9] and the BNL relativistic heavy ion collider (RHIC) [10,11]. The basic finding is that the fluctuations are larger than those expected for uncorrelated particle production.

There are a number of collision characteristics that can be inferred from experimental data on event-by-event fluctuations. First of all, the fluctuation analysis can help to resolve the long-standing problem whether, or rather to what extent, the strongly interacting matter, emerging from the early collision stage, achieves both thermal [12–14] and chemical [15,16] equilibrium. In the NA49 investigation of eventwise fluctuations in the K/π ratio [7] in central Pb+Pb collisions at 158 *A*GeV, no significant deviations from the hadrochemical equilibrium ratio were found. If the equilibrium is indeed reached, the system's heat capacity [17,18] and its compressibility [19] can, in principle, be deduced from the temperature and multiplicity fluctuations, respectively. While large multiplicity fluctuations can be treated as a signal of particle production via clusters [20] or supercooled droplets of deconfined matter [21], small final state fluctuations of the conserved charges, electric or baryonic, can occur when fluctuations generated in the plasma phase are frozen due to the rapid expansion of the system [22,23]. On the other hand, significant transverse momentum and multiplicity fluctuations can result if the system hadronizes from a QGP near the predicted second order critical QCD end point [18,24]. The latter has been shown by recent lattice QCD studies to occur at a substantial baryochemical potential [25], characteristic of the CERN SPS energy range.

The results of fluctuation and correlation measurements can be significantly affected by the acceptance coverage of the detector. The size of this bias in general depends on the nature of the underlying dynamics. Therefore, care has to be taken to compare results from different experiments and from model calculations under similar experimental conditions, such as kinematic acceptance of particles used in the analysis and selected centrality of the collisions.

This paper extends the previous study [6] of the NA49 experiment of event-by-event transverse momentum fluctuations. The main objective is to observe how the fluctuation pattern changes with increasing number of nucleons participating in a collision, i.e., with the system size. For this purpose, not only Pb+Pb collisions at various centralities are studied, but also p+p, C+C, and Si+Si interactions at a beam energy of 158 GeV per nucleon. In particular, it will be checked whether the correlations present in the final state of p+p interactions survive in the collisions of heavier systems, as expected if the nucleus+nucleus (A+A) collision is a simple superposition of nucleon+nucleon (N+N) interactions. Moreover, a test will be performed of the reasonable expectation that the fluctuations become more similar to those of an equilibrated system when the number of participating nucleons increases.

When measuring event-by-event fluctuations in A+A collisions, one should consider the influence of two trivial sources of fluctuations. The first one is caused by event-by-event fluctuations of the collision geometry and the second one by the finite number of particles (statistical fluctuations). The dynamical fluctuations of interest have to be extracted from the noise caused by these trivial sources.

In such a situation, a suitable choice of statistical tools for the study of event-by-event fluctuations is really important. In this work, mainly the fluctuation measure Φ introduced in [12] will be employed. However, other fluctuation measures have also been proposed and studied, e.g., $\sigma_{p_T,dyn}$ [26], $\Delta\sigma_{p_T}$ [27], and Σ_{p_T} [28]; these measures are in fact interrelated. The Φ value is expected to be zero when interparticle correlations are absent. It also eliminates "geometrical" fluctuations due to the impact parameter variation. Thus, Φ is "deaf" to the statistical noise and "blind" to the collision centrality. The Φ measure was already used in the previous experimental study [6] of p_T fluctuations. It was also calculated within various models of nuclear collisions [29–34]. However, in these model considerations, the effects of experimental acceptance were usually not taken into account. Consequently, most of these results cannot be compared to the data.

For better understanding of the structure of the correlations contributing to Φ, two-particle transverse momentum correlations (as proposed in [27]) are studied as well. A preliminary analysis was presented in [35].

This paper is organized as follows: In Sec. II the statistical tools used in this analysis are introduced and briefly discussed. The experimental setup and procedures are presented in Sec. III. Experimental effects such as detector acceptance and two-track resolution are discussed in Sec. IV. The results on the system dependence of the p_T fluctuations are presented in Sec. V. Discussion of the results and their comparison with theoretical models is given in Sec. VI. A summary closes the paper.

II. MEASURES OF FLUCTUATIONS

There are numerous observables that can be used to measure p_T fluctuations in high energy collisions. A natural one is the distribution of the average transverse momentum of the events defined as

$$M(p_T) = \frac{1}{N}\sum_{i=1}^{N} p_{Ti}, \tag{1}$$

where N is the multiplicity of accepted particles in a given event and p_{Ti} is the transverse momentum of the ith particle. The distribution of $M(p_T)$ is usually compared to the corresponding distribution obtained for "mixed events" in which the particles are independent from each other and follow the experimental inclusive spectra (the multiplicity distribution for mixed events is the same as for the data). A difference between the two distributions signals the presence of dynamical fluctuations. Since the $M(p_T)$ distribution crucially

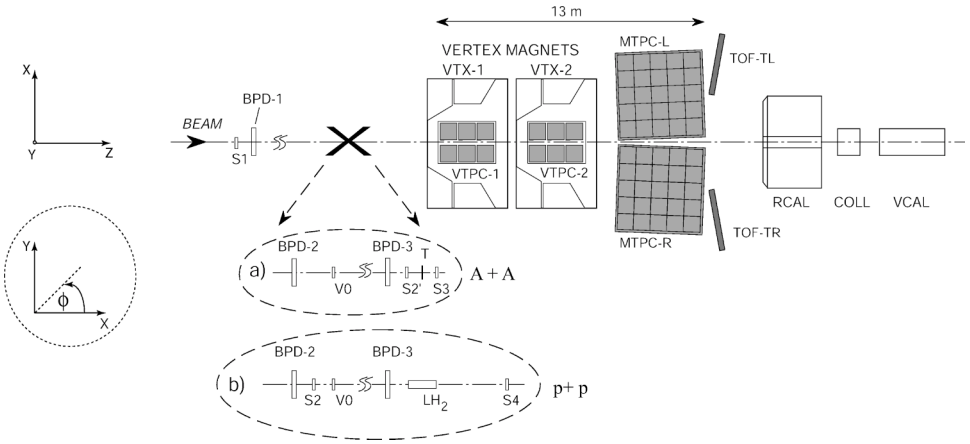

FIG. 1. The experimental setup of the NA49 experiment [38] with different beam definitions and target arrangements.

depends on the particle multiplicity, the method cannot be used to compare systems of significantly different multiplicities.

A more appropriate measure is the quantity Φ [12] which, by its construction, is insensitive to the system size. In this paper the Φ measure is used for the analysis of p_T fluctuations (Φ_{p_T}). Following the authors of [12], one defines the single-particle variable $z_{p_T}=p_T-\overline{p_T}$, with the bar denoting averaging over the single-particle inclusive distribution. One easily observes that $\overline{z_{p_T}}=0$. Further, one introduces the event variable Z_{p_T}, which is a multiparticle analog of z_{p_T}, defined as

$$Z_{p_T}=\sum_{i=1}^{N}(p_{Ti}-\overline{p_T}), \tag{2}$$

where the summation runs over particles in a given event. Note that $\langle Z_{p_T}\rangle=0$, where $\langle\ldots\rangle$ represents averaging over events. Finally, the Φ_{p_T} measure is defined as

$$\Phi_{p_T}=\sqrt{\frac{\langle Z_{p_T}^2\rangle}{\langle N\rangle}}-\sqrt{\overline{z_{p_T}^2}}. \tag{3}$$

The second part of Eq. (3) is simply the dispersion of the inclusive p_T distribution (further denoted as σ_{p_T}). It can be easily shown that $\Phi_{p_T}=0$, when no interparticle correlations are present and the single-particle spectrum is independent of multiplicity. As already mentioned, Φ_{p_T} is insensitive to centrality. This property may be expressed as follows: Φ_{p_T} is independent of the distribution of the number of particle sources if the sources are identical and independent from each other [12,14]. In particular, Φ_{p_T} does not depend on the impact parameter if the A+A collision is a simple superposition of N+N interactions.

In spite of the abovementioned advantages, there is an important disadvantage of using Φ_{p_T} in the fluctuation analysis. While Φ_{p_T} is sensitive to the presence of dynamical correlations in a system, it does not disentangle their nature. Fluctuations of very different character contribute to Φ_{p_T}. In order to achieve a better understanding of the fluctuation structure, one needs to apply a more differential method [27].

The correlations can be studied by plotting the cumulative p_T variables of particle pairs. Namely, for a given particle, instead of its p_T one introduces the variable x defined as [36]

$$x(p_T)=\int_0^{p_T}\rho(p_{T'})dp_{T'}, \tag{4}$$

where $\rho(p_T)$ is the inclusive p_T distribution, normalized to unity, which is obtained from all particles used in the analysis. By construction, the x variable varies between 0 and 1 with a *flat* probability distribution. The two-particle correlation plots, as presented in this paper, are obtained by plotting (x_1,x_2) points for all possible particle pairs within the same event. The number of pairs in each (x_1,x_2) bin is divided by the mean number of pairs in a bin [averaged over all (x_1,x_2) bins]. This two-dimensional plot is uniform when no interparticle correlations are present in the system. Correlations due to the Bose statistics produce a ridge along the diagonal of the (x_1,x_2) plot, which starts at $(0,0)$ and ends at $(1,1)$, whereas temperature fluctuations lead to a saddle shaped structure [27].

As will be seen in the figures, the distribution of x_1 or x_2 obtained from the two-dimensional (x_1,x_2) plots by projecting on the x_1 or x_2 axis is not flat. This is due to the method by which the plots are constructed. Namely, each pair of particles is represented by a point on the plot. Therefore, the events with higher multiplicities are represented by a larger number of pairs than those with smaller multiplicities. Since the shape of the p_T distribution depends on the event multiplicity, the projection of the two-dimensional plot on x_1 or x_2 is no longer flat. However, it should be stressed that in the absence of any correlations the (x_1,x_2) plot is uniformly populated and the x_1 and x_2 projections are flat.

III. EXPERIMENTAL SETUP

The NA49 experiment is a large acceptance hadron spectrometer at the CERN-SPS used to study the hadronic final states produced by collisions of various beam particles (p, Pb from the SPS and C, Si from the fragmentation of the primary Pb beam) with a variety of fixed targets. The main tracking devices are four large-volume time projection chambers (TPCs) (Fig. 1), which are capable of detecting 80% of

approximately 1500 charged particles created in a central Pb+Pb collision at 158 *A*GeV. Two of them, the vertex TPCs (VTPC-1 and VTPC-2), are located in the magnetic field of two superconducting dipole magnets (1.5 and 1.1 T, respectively) and two others (MTPC-L and MTPC-R) are positioned downstream of the magnets symmetrically to the beam line. The results presented here are analyzed with a global tracking scheme [37], which combines track segments that belong to the same physical particle but which were detected in different TPCs. The NA49 TPCs allow precise measurements of particle momenta p with a resolution of $\sigma(p)/p^2 \cong (0.3-7)\times 10^{-4}$ (GeV/c)$^{-1}$. The setup is supplemented by two time of flight detector arrays and a set of calorimeters.

The targets, C (561 mg/cm^2), Si (1170 mg/cm^2), and Pb (224 mg/cm^2) for ion collisions and a liquid hydrogen cylinder (length 20 cm) for elementary interactions, are positioned about 80 cm upstream from VTPC-1.

Pb-beam particles are identified by means of their charge as seen by a helium gas cherenkov counter (S2') and p-beam particles by a 2 mm scintillator (S2). Both of these are situated in front of the target. The study of C+C and Si+Si reactions is possible through the generation of a secondary fragmentation beam that is produced by a primary target (1 cm carbon) in the extracted Pb beam. With the proper setting of the beam line magnets, a large fraction of all $Z/A=1/2$ fragments at $\approx$158 *A*GeV are transported to the NA49 experiment. On-line selection based on a pulse height measurement in a scintillator beam counter (S2) is used to select particles with $Z=6$ (Carbon) and $Z=13,14,15$ (Al, Si, P). In addition, a measurement of the energy loss in beam position detectors (BPD-1/2/3 in Fig. 1) allows for a further selection in the off-line analysis. These detectors consist of pairs of proportional chambers and are placed along the beam line. They also provide a precise measurement of the transverse positions of the incoming beam particles.

For p, C, and Si beams, interactions in the target are selected by an anti-coincidence of the incoming beam particle with a small scintillation counter (S4) placed at the beam axis between the two vertex magnets. For p+p interactions at 158 *A*GeV, this counter selects a (trigger) cross section of 28.5 mb out of 31.6 mb of the total inelastic cross section. For Pb beams, an interaction trigger is provided by an anti-coincidence with a helium gas Cherenkov counter (S3) directly behind the target. The S3 counter is used to select minimum bias collisions by requiring a reduction of the Cherenkov signal by a factor of about 6. Since the Cherenkov signal is proportional to Z^2, this requirement ensures that the Pb projectile has interacted with a minimal constraint on the type of interaction. This setup limits the triggers on non-target interactions to rare beam-gas collisions, the fraction of which proved to be small after cuts, even in the case of peripheral Pb+Pb collisions.

The centrality of the nuclear collisions is selected by use of information from a downstream calorimeter (VCAL), which measures the energy of the projectile spectator nucleons. The geometrical acceptance of the VCAL calorimeter is adjusted in order to cover the projectile spectator region by the setting of the collimator (COLL).

Details of the NA49 detector setup and performance of tracking software are described in [38].

TABLE I. Data sets used in analysis. Listed for p+p, C+C, Si+Si, and six centralities of Pb+Pb collisions at 158 *A*GeV are: number of events; σ/σ_{tot}, the fraction of the total inelastic cross section in that bin; $\langle N_W\rangle$, the mean number of wounded nucleons; and b, the impact parameter range.

	No. of events	σ/σ_{tot} in each bin	$\langle N_W\rangle$	b range [fm]
p+p	570 000	0.9	2	
C+C	33 000	0.153	14	0–2.0
Si+Si	63 000	0.122	37	0–2.6
Pb+Pb(6)	117 000	0.57	42	10.2–
Pb+Pb(5)	59 000	0.10	88	9.1–10.2
Pb+Pb(4)	68 000	0.10	134	7.4–9.1
Pb+Pb(3)	68 000	0.11	204	5.3–7.4
Pb+Pb(2)	45 000	0.075	281	3.4–5.3
Pb+Pb(1)	180 000	0.05	352	0–3.4

IV. DATA SELECTION AND ANALYSIS

A. Data sets

The data used for the analysis consists of samples of p+p, C+C, Si+Si, and Pb+Pb collisions at 158 *A*GeV. For Pb+Pb interactions a minimum bias trigger was used allowing a study of the centrality dependence. The distribution of energy measured in the VCAL for the minimum bias Pb+Pb events was divided into six centrality bins (Table I), which are numbered from 1 (the most central) to 6 (the most peripheral). For each bin of centrality, the range of the impact parameter b and the mean number of wounded nucleons $\langle N_W\rangle$ were determined by use of the Glauber model and the VENUS event generator [39]. The fraction of the total inelastic cross section of nucleus+nucleus collisions (σ/σ_{tot}) corresponding to each data set was obtained directly by use of the distribution of energy measured in the VCAL. In order to estimate the correlation between the energy deposited in the VCAL and the impact parameter minimum bias, VENUS events were processed through the GEANT detector simulation code, and the energy deposited in the VCAL was simulated. The correlation between b and $\langle N_W\rangle$ was obtained from Glauber model calculations using the spectator-participant model of A+A interactions. The values of σ/σ_{tot}, $\langle N_W\rangle$, and b presented in Table I are taken from [40] for minimum bias Pb+Pb collisions and from [41] for C+C and Si+Si interactions.

The minimum bias Pb+Pb data consists of data taken during three different periods and at both magnetic field polarities. The most central Pb+Pb events correspond to 5% of the total geometric cross section. Since the minimum bias data provide only a small number of events in the most central Pb+Pb bin, additional central trigger runs were used.

B. Event and particle selection

The aim of the event selection criteria is to reduce a possible contamination with nontarget collisions. The primary vertex was reconstructed by fitting the intersection point of the measured particle trajectories. Only events with a proper

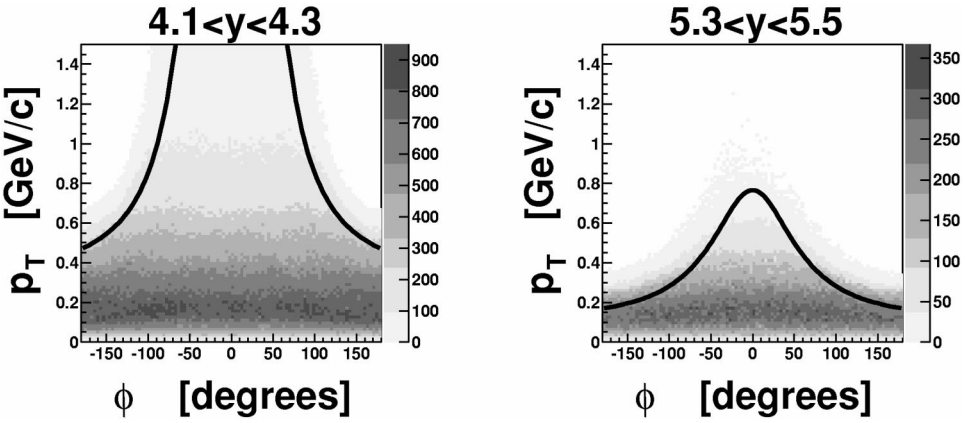

FIG. 2. NA49 $\phi - p_T$ acceptance of positively charged particles (standard configuration of magnetic field) for two selected rapidity bins at 158 *A*GeV. The solid lines represent the analytical parametrization.

quality and position of the reconstructed vertex are accepted in this analysis. The vertex coordinate z along the beam has to satisfy $|z-z_0|<\Delta z$, where the nominal vertex position z_0 and cut parameter Δz values are: −579.5 and 5.5 cm, −579.5 and 1.5 cm, −579.5 and 0.8 cm, and −578.9 and 0.4 cm for p+p, C+C, Si+Si, and Pb+Pb collisions, respectively.

In order to reduce the contamination of particles from secondary interactions, weak decays and other sources of nonvertex tracks, several track cuts are applied. The accepted particles are required to have measured points in at least one of the VTPCs. A cut on the so-called track impact parameter, the distance between the reconstructed main vertex and the track in the target plane, is applied ($|b_x|<2$ cm and $|b_y|<1$ cm) to reduce the contribution of nonvertex particles. Moreover, particles are accepted only when the potential number of points (calculated on the basis of the geometry of the track) in the detector exceeded 30. The ratio of the number of points on a track to the potential number of points is required to be higher than 0.5 in order to avoid the counting of track segments instead of whole tracks. Only forward rapidity tracks ($4.0<y_\pi<5.5$, rapidity calculated assuming the pion mass for all particles) with $0.005<p_T<1.5$ GeV/c are used in this analysis. The above y_π and p_T cuts imply that rapidities of the selected kaons and protons range from 2.7 to 5.0 and from 2.5 to 5.0, respectively. Note that the center of mass rapidity in the laboratory system is 2.91 at 158 *A*GeV.

The NA49 detector provides a large (but not complete) acceptance in the forward hemisphere. Two example plots of p_T versus azimuthal angle ϕ (see Fig. 1 for definition) for positively charged particles (for the standard polarity of the magnetic field) are shown in Fig. 2. The solid lines represent a parametrization of the acceptance limits by the formula

$$p_T(\phi) = \frac{1}{A + \phi^2/C} + B, \tag{5}$$

where the values of parameters A, B, and C depend on the rapidity interval as given in Table II. These values apply to negatively charged particles as well, provided ϕ in Eq. (5) is replaced by $\mathrm{sign}(\phi)\cdot(180-\phi)$. Only particles within the analytical curves are used in this analysis. This well-defined acceptance is essential for later comparison of the results with models and other experiments.

The NA49 detector is able to register particles produced in a significantly wider rapidity range covering almost the whole forward hemisphere. It would be interesting to determine the correlation measure Φ_{p_T} in the mid-rapidity region. Preliminary results for the rapidity range 2.9–4.0 were reported [42]. However, the azimuthal acceptance in this region is more limited and systematic uncertainties affecting Φ_{p_T} are not yet fully understood.

C. Corrections and error estimates

The statistical error on Φ_{p_T} was estimated as follows. The whole sample of events was divided into 30 subsamples. The value of Φ_{p_T} was evaluated for each subsample and the dispersion (D) of the results was then calculated. The statistical error of Φ_{p_T} was taken to be equal to $D/\sqrt{30}$.

The event and track selection criteria reduce the possible systematic bias of the measured Φ_{p_T} values. In order to estimate the remaining systematic uncertainty, the values of cut parameters have been varied within a reasonable range and the systematic error has been estimated as a half of the difference between the highest and the lowest Φ_{p_T} value. In addition, results obtained from the analysis of data taken at two different magnetic field polarities as well as from different running periods have been compared.

TABLE II. The parametrization of the NA49 $y-p_T$ acceptance at 158 *A*GeV for positively charged particles (standard configuration of magnetic field). For negatively charged particles, one has to redefine the azimuthal angle and then use the same parametrization.

y_π	$A\left[\frac{c}{\mathrm{GeV}}\right]$	$B\left[\frac{\mathrm{GeV}}{c}\right]$	$C\left[\frac{\mathrm{deg}^2\mathrm{GeV}}{c}\right]$
3.9–4.1	0	0.3	6500
4.1–4.3	0	0.3	5500
4.3–4.5	0	0.25	4500
4.5–4.7	0	0.25	3500
4.7–4.9	0	0.2	2500
4.9–5.1	0.5	0.2	2500
5.1–5.3	1.0	0.1	2500
5.3–5.5	1.5	0.1	2500

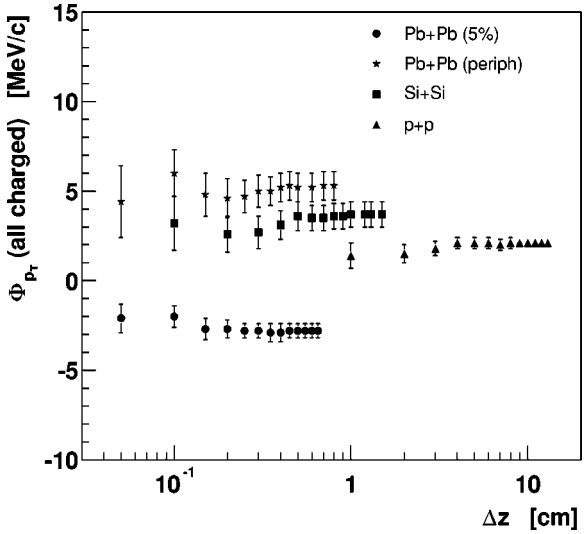

FIG. 3. The dependence of Φ_{p_T} on the allowed distance Δz of the reconstructed event vertex from its nominal position. Note: the values and their errors are correlated.

Event cuts are used to reject possible contamination of nontarget interactions, however, there is always a small fraction of remaining nontarget events that can influence the Φ_{p_T} values. The dependence of Φ_{p_T} on the event selection cut Δz is shown in Fig. 3. The observed variation of Φ_{p_T} with Δz is small. The estimated systematic error is smaller than 0.85 MeV/c for peripheral Pb+Pb collisions, 0.55 MeV/c for Si+Si data, and 0.5 MeV/c for p+p events.

The majority of tracks selected by the track selection criteria are main vertex tracks and the remaining fraction ($\approx$10%) originates predominantly from weak decays and secondary interactions with the material of the detector. In order to estimate the influence of this contamination on the measured value of Φ_{p_T}, the impact parameter cut was varied (Fig. 4). A small increase of Φ_{p_T} with increasing impact parameter cut is observed and may be due to the increased contribution of nonvertex tracks from weak decays and secondary interactions. A direct estimate of the effect of nonvertex tracks was obtained by use of events from the VENUS event generator [39]. After full detector simulation and reconstruction by the standard program chain, it was found that for central Pb+Pb collisions, where the bias is the largest, the value of Φ_{p_T} decreases by about 1 MeV when nonvertex tracks (about 12% of all accepted) are excluded from the analysis. The estimated systematic error due to the contamination of nonvertex tracks (resulting from Fig. 4) is smaller than 1.6 MeV/c for central Pb+Pb collisions, 0.75 MeV/c for Si+Si data, and 0.35 MeV/c for p+p events.

Losses of tracks due to the reconstruction inefficiency and track selection cuts influence the measured Φ_{p_T} values. In order to estimate this effect, the dependence of Φ_{p_T} on the percentage of randomly rejected particles was calculated. These dependences for the most peripheral (6), the most central (1) Pb+Pb collisions and for p+p interactions are shown in Fig. 5. Within the considered kinematic region (forward rapidity) the tracking efficiency of our detector is higher than 95%. Figure 5 implies that the bias due to tracking inefficiency is not higher than 0.5–1.0 MeV/c.

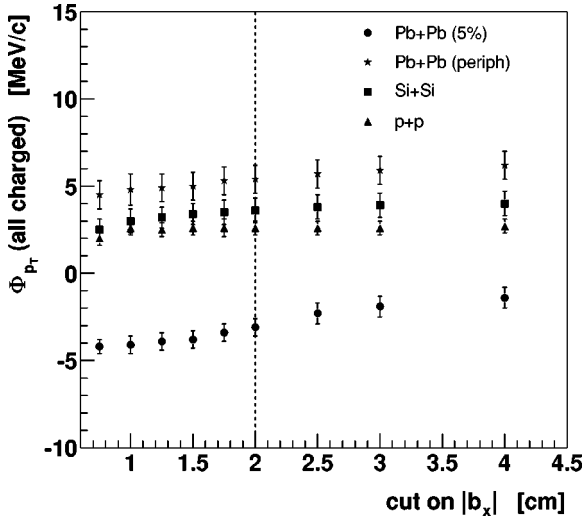

FIG. 4. The dependence of Φ_{p_T} on the upper cut in the impact parameter $|b_x|$. For each point, the cut on $|b_y|$ was equal half the cut on $|b_x|$. Note: the values and their errors are correlated. The dashed line indicates the cut used in the analysis.

As an estimate of the systematic error on Φ_{p_T} a maximal error resulting from the above study has been taken. The systematic error is about 1.6 MeV/c for Pb+Pb collisions and 1.2 MeV/c for p+p, C+C, and Si+Si interactions.

It has already been shown [6] that the limited two-track resolution influences the measured Φ_{p_T} values. In order to estimate this contribution, several samples of mixed events (for different A+A collisions) were produced. Mixed events were constructed from original events, the multiplicities of mixed events being the same as in the case of real events but each particle in a mixed event taken at random from a different real event. The Φ_{p_T} value calculated for the sample of mixed events was consistent with zero. In the second step, the mixed events were processed by the NA49 simulation software. The resulting simulated raw data were reconstructed and the Φ_{p_T} measure calculated. The obtained Φ_{p_T}

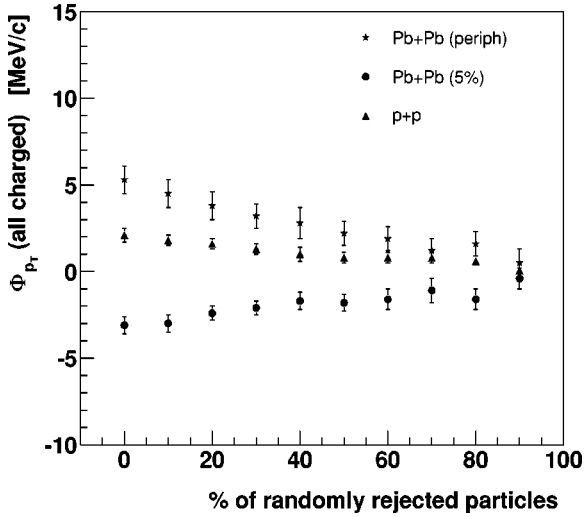

FIG. 5. The dependence of Φ_{p_T} on the fraction of randomly rejected particles.

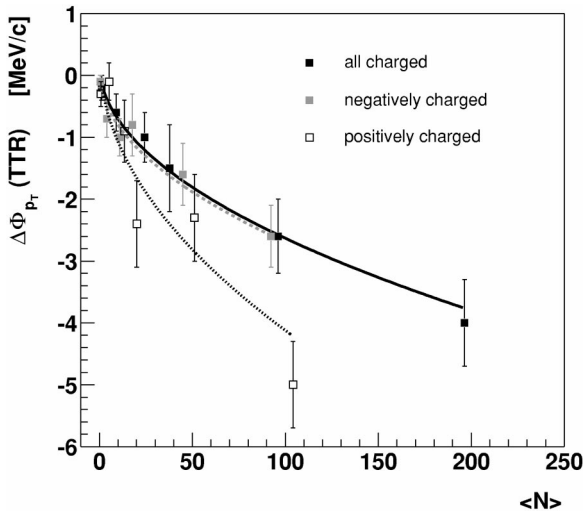

FIG. 6. Additive correction $\Delta\Phi_{p_T}$ for limited two-track resolution effect versus multiplicity $\langle N\rangle$ of accepted particles. Different points correspond to positively charged, negatively charged, and all charged particles. The presented corrections have been determined using p+p, C+C, Si+Si, and three centralities of Pb+Pb collisions at 158 *A*GeV. The lines represent the analytical parametrization: $\Delta\Phi_{p_T}(\langle N\rangle) = -a\sqrt{\langle N\rangle} + b$ with a and b being parameters of a fit to the data points.

values are negative as expected for the anti-correlation introduced by the losses due to the limited two-track resolution. The additive two-track resolution correction is calculated as the difference ($\Delta\Phi_{p_T}$) between the values of Φ_{p_T} after and before this procedure. Figure 6 presents this correction versus mean multiplicity. The lines correspond to an analytical parametrization of this dependence. The absolute values of the track resolution corrections are larger for heavier colliding systems where the density of tracks is relatively high. The absolute values of $\Delta\Phi_{p_T}$ are also larger for positively charged particles than for negatively charged ones, which is mainly due to higher track density for positive particles caused by significantly larger number of protons than antiprotons. The $\Delta\Phi_{p_T}$ values are negative, indicating that Φ_{p_T} measured with an ideal detector would be higher. For a given multiplicity, Φ_{p_T} corrected for the limited two-track resolution effect equals "raw" Φ_{p_T} minus the corresponding $\Delta\Phi_{p_T}$. The error of the corrected Φ_{p_T} was calculated by adding in squares the statistical error of the raw Φ_{p_T} value and the statistical error of the correction.

V. RESULTS

The results shown in this section refer to *accepted* particles, i.e., particles that are accepted by the detector and pass all kinematic cuts and track selection criteria. The data cover a broad range in p_T ($0.005 < p_T < 1.5$ GeV/c). The rapidity of accepted particles is restricted to the interval 4.0 to 5.5, which corresponds to forward rapidities in the collision of equal mass nuclei (at 158 *A*GeV energy the center of mass rapidity equals 2.9 for fixed target geometry), where the azimuthal acceptance is large.

The mean multiplicities of accepted particles, the dispersions $\sigma_N = \sqrt{\langle N^2\rangle - \langle N^2\rangle}$ of the multiplicity distributions, the mean inclusive transverse momenta, the dispersions σ_{p_T} of inclusive transverse momentum distributions and Φ_{p_T} values for all data sets used in this analysis are given in Table III. The Φ_{p_T} values shown in this table have been calculated for all accepted charged particles as well as for the negatively and the positively charged particles separately. All values of Φ_{p_T} were corrected for the two-track resolution effect.

Figure 7 shows the distributions of the mean (per event) transverse momentum $M(p_T)$ for p+p, Si+Si and central Pb+Pb collisions. Points correspond to data and the histograms to mixed events. The data are not corrected for any experimental effects. Events with zero accepted particle multiplicity are not taken into account. The small difference between $M(p_T)$ distributions for real and mixed events demonstrates that dynamical fluctuations are small. Moreover, no distinct class of events with unusual fluctuations is observed. The width of the $M(p_T)$ distribution strongly decreases with the colliding system size as expected from the increasing particle multiplicity.

The fluctuation measure Φ_{p_T} is more sensitive to small dynamical fluctuations. The measured values, corrected for two-track resolution, are plotted in Fig. 8 versus mean number of wounded nucleons for all accepted charged particles and also for positively and negatively charged particles separately. The Φ_{p_T} values are small (when compared to σ_{p_T}) for all investigated systems ($|\Phi_{p_T}| < 10$ MeV/c), but a significant centrality dependence is observed. The Φ_{p_T} values increase by about 5 MeV from p+p collisions up to the maximum value, which is observed for the most peripheral Pb+Pb collisions, and then Φ_{p_T} values decrease with increasing number of wounded nucleons. The statistical significance of this decrease can be estimated to be about 5.5, 4.6, and 4.5 σ for all charged, negatively charged, and positively charged hadrons, respectively. The effect was found to be stable with respect to the variation of the track selection cuts. The Φ_{p_T} value for Si+Si collisions seems to be lower than that for the most peripheral Pb+Pb ones although the number of wounded nucleons in both reactions is similar. This might suggest that $\langle N_W\rangle$ does not fully determine the fluctuations in A+A collisions. The Φ_{p_T} measure calculated for positively charged particles is lower than that for the negatively charged ones. However, the measured difference of about 2–3 MeV/c is comparable with the systematic error. The Φ_{p_T} value for all charged particles seems to be higher than that for the negatively charged particles.

Two-particle correlation plots of the cumulant transverse momentum variable x are presented in Fig. 9 for p+p, C+C, Si+Si, and three centralities of Pb+Pb interactions (note the different color scales). It is seen that the plots are not uniformly populated. In particular, significant long range correlations of about 40% (the color scale varies from 0.75 to 1.6) are observed for the p+p data. This is rather unexpected when compared to the low Φ_{p_T} value. These correlations are not seen when heavier colliding systems are studied. Instead, short range correlations become visible as an enhancement of the point density in the region close to the diagonal. They are

TABLE III. Measured inclusive and event-by-event parameters for accepted particles. $\langle N \rangle$, σ_N, $\overline{p_T}$, and σ_{p_T} values are not corrected for acceptance. Φ_{p_T} values are corrected for limited two-track resolution. The systematic errors of Φ_{p_T} are smaller than 1.6 MeV/c.

	$\langle N \rangle$	σ_N	$\overline{p_T}$ [MeV/c]	σ_{p_T} [MeV/c]	Φ_{p_T} [MeV/c]
p+p (all)	1.4	1.3	304	196	2.2±0.3
p+p(−)	0.6	0.7	283	179	0.8±0.1
p+p(+)	0.8	0.9	317	206	−1.4±0.3
C+C (all)	10	4.3	300	210	5.4±0.7
C+C(−)	4.5	2.4	279	190	1.8±0.8
C+C(+)	5.5	2.7	317	224	0.7±0.7
Si+Si (all)	27	7	301	217	4.9±0.8
Si+Si (−)	12	4	277	195	2.6±0.5
Si+Si(+)	15	4	320	231	−0.2±0.7
Pb+Pb(6) (all)	39	18	299	220	7.2±0.7
Pb+Pb(6)(−)	18	9	270	195	4.5±0.5
Pb+Pb(6)(+)	21	10	325	237	1.9±0.7
Pb Pb(5) (all)	73	17	305	226	6.6±0.7
Pb+Pb(5)(−)	34	9	273	199	4.5±0.7
Pb+Pb(5)(+)	39	9	333	245	0.6±0.8
Pb+Pb(4)(all)	104	19	309	230	5.6±0.8
Pb+Pb(4)(−)	49	10	276	202	3.8±0.5
Pb+Pb(4)(+)	55	11	337	249	−0.6±0.9
Pb+Pb(3) (all)	148	21	312	233	4.6±0.8
Pb+Pb(3)(−)	69	11	279	204	2.9±0.8
Pb+Pb(3)(+)	79	12	342	252	−1.3±0.8
Pb+Pb(2) (all)	193	21	315	234	2.2±1.0
Pb+Pb(2) (−)	90	11	281	205	2.4±0.8
Pb+Pb(2)(+)	103	13	344	254	−3.7±1.1
Pb+Pb(1) (all)	230	19	317	236	1.4±0.8
Pb+Pb(1)(−)	108	11	281	203	0.9±0.6
Pb+Pb(1)(+)	122	12	349	257	−2.9±0.8

most prominent for central Pb+Pb collisions and are consistent with the effect of Bose-Einstein statistics. For the most peripheral collisions the pattern seen in the two-particle correlation plot is different from that in the remaining systems. One observes an enhancement in the region close to $x_1=1$ and $x_2=1$.

VI. DISCUSSION

Figure 8 shows that Φ_{p_T} is a nonmonotonic function of centrality with the maximum at approximately $N_W=40$. Such a behavior strongly resembles the dependence of the magnitude of collective flow—directed (v_1) and elliptic (v_2)—on N_W [43]. Thus, there is a natural suggestion that the p_T fluctuations measured by Φ_{p_T} may be caused by the collective flow. This suggestion was checked by performing a simple Monte Carlo analysis generating events with independent particles, following the measured inclusive p_T distribution. The uniform azimuthal angle distribution of the events was modified by the collective elliptic flow, but the particles remained independent from each other with respect to their transverse momenta. For such events, the dynamical p_T fluctuations vanish if the azimuthal angle acceptance is complete. However, the azimuthal angle acceptance of the NA49 detector is not flat, and consequently the azimuthal anisotropy generates a finite value of Φ_{p_T}, even though the p_T of particles are independent of each other. In order to quantify the effect, a simple simulation was performed in which elliptic flow was the only source of particle correlations. In these calculations, the v_2 dependence on transverse momentum was parametrized as $v_2=0.05\ p_T(\mathrm{GeV/c})$ according to the previous NA49 measurements [43]. The resulting Φ_{p_T} value is 0.0±0.6 MeV/c. Thus, one concludes that the effect of the azimuthal anisotropy caused by the collective flow combined with the incomplete azimuthal acceptance is not responsible for the observed dynamical p_T fluctuations. Finally, we checked that only the abnormally large value of $v_2=0.5$ leads to Φ_{p_T} as large as 17 MeV/c.

In Fig. 10 the dependence of Φ_{p_T} on the mean number of wounded nucleons is directly compared to predictions of the HIJING [44] model (default parameters were used) for all charged particles, and for negatively charged and positively

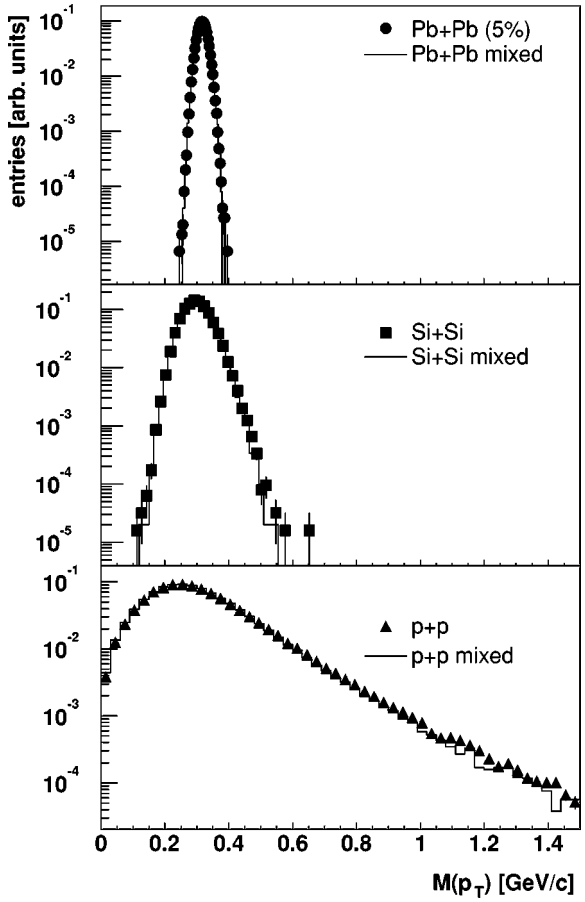

FIG. 7. Distributions of mean transverse momentum for real (data points) and mixed events (histograms). Data points are not corrected for acceptance and limited two track resolution. Events with accepted particle multiplicity equal to zero are not used.

charged particles separately. The same kinematic cuts are applied as for the data. The black lines represent the results of the HIJING simulations where the effect of the limited NA49 acceptance (p_T versus azimuthal angle) is taken into account. The gray lines refer to the HIJING predictions for full azimuthal acceptance to demonstrate the effect of the limited acceptance of the detector.

In contrast to the data, Φ_{p_T} computed within the HIJING model does not change when going from elementary to central Pb+Pb collisions because the HIJING model represents an essentially independent superposition of N+N interactions. The effects of short range correlations (Bose-Einstein and Coulomb) have not been incorporated in the HIJING model. However it was estimated in the previous analysis [6] that the combined effect of short range correlations produces Φ_{p_T} values on the level of 5 MeV/c for central Pb+Pb collisions. This effect strongly depends on multiplicity and becomes negligible for p+p interactions.

For the HIJING model, Φ_{p_T} values for positively charged particles are, as in the case of real data, lower than for negatively charged and for all charged particles. Within the HIJING model, the fact that Φ_{p_T} values for positively charged particles are always lower than for negatively charged ones has been found to be related to the limited

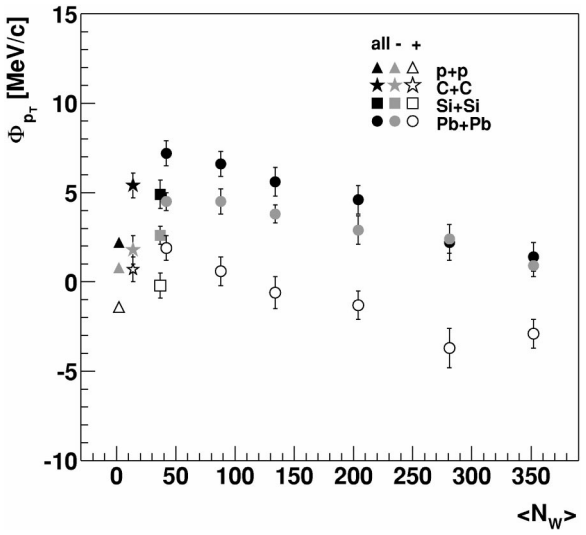

FIG. 8. Φ_{p_T} versus mean number of wounded nucleons $\langle N_W \rangle$. Data points were corrected for limited two-track resolution. Errors are statistical only. Systematic error is smaller than 1.6 MeV/c.

acceptance and a contribution of protons in the sample of positively charged hadrons.

When Φ_{p_T} was first introduced [12], it was believed that its value would be nonzero for elementary interactions [mainly due to the $M(p_T)$ versus N dependence] and would vanish for heavier colliding systems as a result of equilibration. The present measurements do not confirm this expectation. Although Φ_{p_T} is close to zero for central Pb+Pb collisions, the maximum value is observed not for p+p data, but for colliding systems with $N_W \simeq 40$.

Although the value of Φ_{p_T} is small for p+p collisions, a significant structure appears in the two-particle correlation plot (Fig. 9). The first candidate for its origin is the dependence of $M(p_T)$ on N, observed for elementary interactions [12]. Figure 11 compares $\langle M(p_T) \rangle$ versus N for the HIJING model and for real p+p data ($\langle \ldots \rangle$ represents averaging over events with a given N). The HIJING model includes the NA49 acceptance and all kinematic restrictions. It shows good agreement with the measurements. Figure 12 presents the p+p two-particle correlation plots for data (a), for the HIJING model (b), and for a simple random generator, which reproduces the dependence of $M(p_T)$ on N observed in the data (c). The accepted particle multiplicity distribution for the random generator (c) is the same as in the case of data (all kinematic cuts and NA49 geometric acceptance are included). Both models (b) and (c) qualitatively reproduce the structure of the two-particle correlation plot observed in the data, however, the HIJING model (b) shows additionally a small enhancement of the point density in the region of high x.

The Φ_{p_T} value calculated for model (c) for all charged particles equals $1.2 \pm 0.2 \pm 1.8$ MeV/c and is consistent with Φ_{p_T} for the p+p data ($2.2 \pm 0.3 \pm 1.2$ MeV/c). Nevertheless, the small difference might indicate that, in agreement with the analysis presented in [33], there could be an additional source of correlations present in the data. However, due to the relatively high statistical and systematic errors the effect

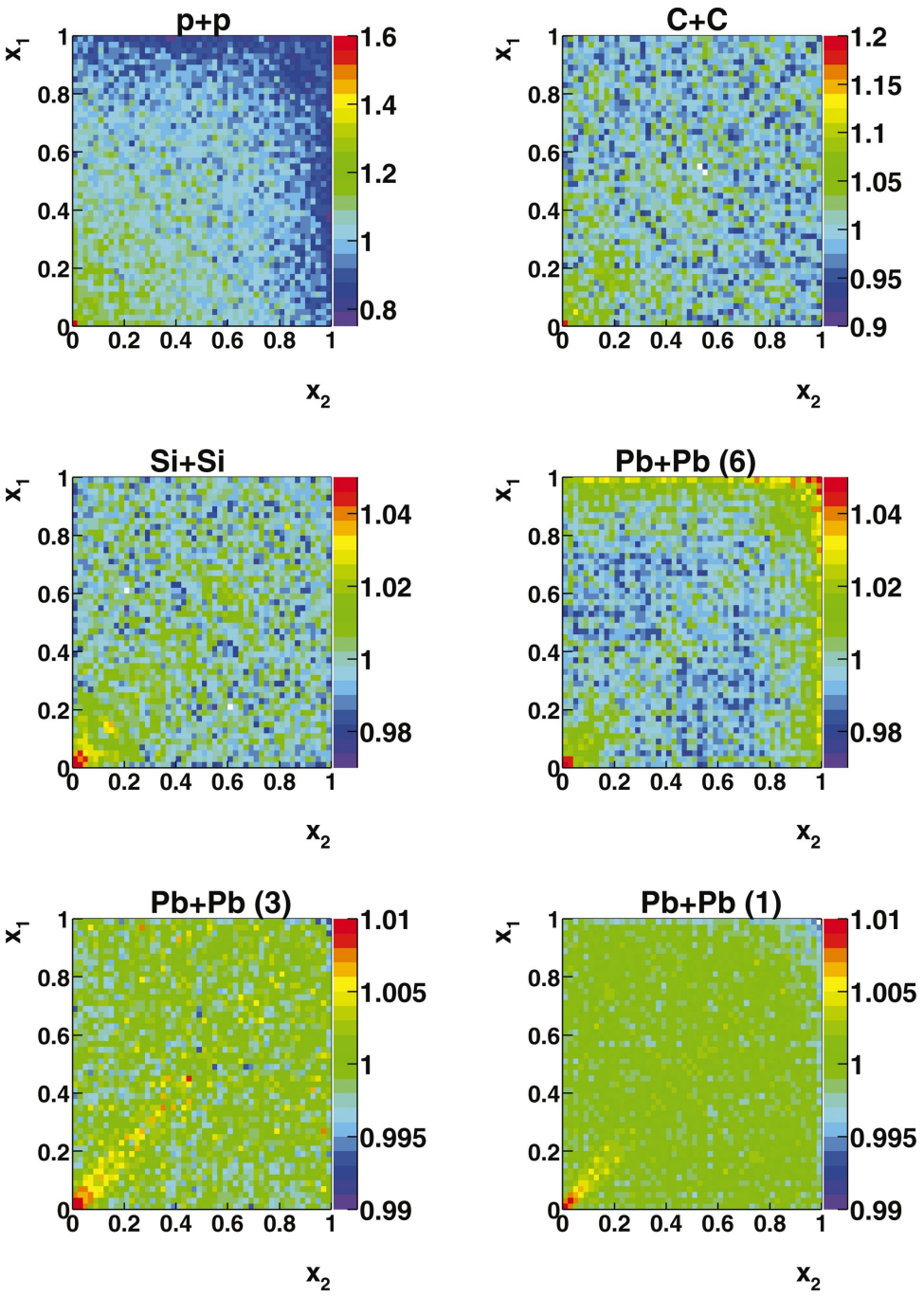

FIG. 9. (Color) Two-particle correlation plots using the cumulant p_T variable x. After each charged particle pair (x_1, x_2) was entered into the plot, the bin contents were normalized by dividing with the average number of entries per bin. The data are plotted with different color scales.

cannot be estimated quantitatively. A similar analysis was carried out for negatively charged particles only, where the correlations caused by resonances and by charge conservation are expected to be smaller than those for all charged particles. There, the experimental value of Φ_{p_T} is $0.8 \pm 0.1 \pm 1.2$ MeV/c, while the model (c) gives $0.6 \pm 0.2 \pm 0.3$ MeV/c. Two-particle correlation plots for negatively charged particles only are very similar for data and for model (c). Thus, one concludes that the results on negative particles from p+p interactions are consistent with the conjecture [45] that the particles are emitted independently, but that their y and p_T distributions depend on event multiplicity.

The last panel (d) of Fig. 12 presents the result of a simple temperature fluctuation model (the concept is described in [34]), which assumes that the only source of fluctuations is event-by-event fluctuation of the inverse slope parameter (T) of the transverse mass spectra. The model assumes a Gaussian shaped rapidity distribution and an exponential shape of the transverse mass distribution with the mean inverse slope parameter $\langle T \rangle = 152$ MeV adjusted to agree with the experimental p+p results. All kinematic cuts applied for the real data are also used in this model and the effect of the finite detector acceptance is taken into account. The mean multiplicity of all accepted particles is the same as in the data. The fluctuations of the inverse slope parameter lead to a saddle

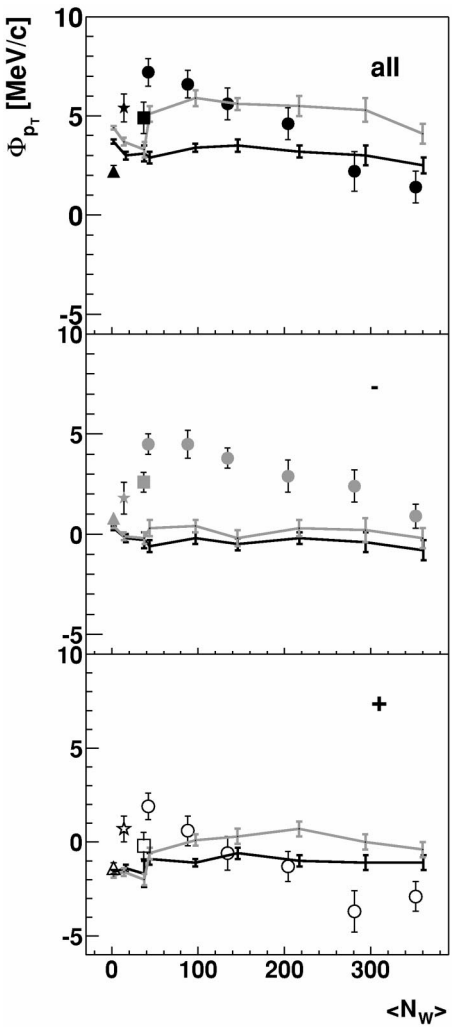

FIG. 10. Φ_{p_T} versus mean number of wounded nucleons calculated using the HIJING model with geometrical acceptance cuts included (black lines) and without geometrical acceptance restrictions (gray lines). Results are compared to data (points) corrected for limited two-track resolution (the markers are the same as in Fig. 8). The panels represent: all charged, negatively charged, and positively charged particles. Data points contain both short and long range correlations. The effects of short range correlations are not incorporated in the HIJING model.

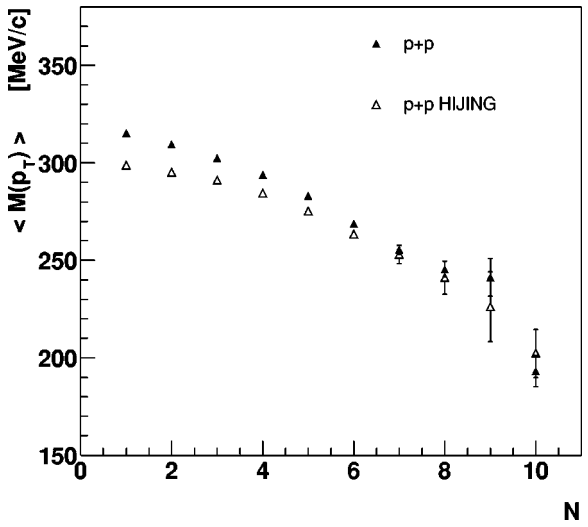

FIG. 11. Mean transverse momentum versus multiplicity of all accepted particles. The closed symbols represent p+p data at 158 *A*GeV (data are not corrected for limited two-track resolution effect) and the open symbols corresponds to p+p events simulated using the HIJING model (the effects of the limited NA49 acceptance are included). Events with accepted particle multiplicity equal to zero are not used.

shaped structure in the two-particle correlation plots. Panel (d) shows the result for fluctuations of T on the level of about 10% (the dispersion $\sigma_T = 16$ MeV), which results in the value of Φ_{p_T} as in the data. Because of the difference between the panels (a) and (d) one concludes that fluctuations of the inverse slope parameter are not the source of correlations in p+p data.

The HIJING model has also been used to obtain a two-particle correlation plot for C+C collisions [Fig. 13(b)], which appears to be similar to that observed for real events (Fig. 9). Figure 13(a) [the same as Fig. 12(b)] presents p+p events simulated by the HIJING model. The structure observed for p+p collisions vanishes for heavier systems due to the dilution effect from the higher number of uncorrelated particles (resulting from different N+N interactions), whereas the Φ_{p_T} measure is not affected by this dilution effect.

In order to see how dynamical fluctuations influence two-particle correlation plots for central Pb+Pb data, the above model with fluctuations of the inverse slope parameter was used again. The mean inverse slope parameter $\langle T \rangle$ was set to 190 MeV and the mean multiplicity of all accepted particles to 200 in order to compare the results with central Pb+Pb collisions. The inverse slope parameter varied from event to event with a Gaussian shaped distribution of width σ_T. Figure 14 presents (x_1, x_2) plots for different levels of the inverse slope parameter fluctuations. The fluctuations lead to a saddle shaped structure which is not visible in central Pb+Pb collisions. One can thus exclude significant T fluctuations in central Pb+Pb collisions at top SPS energy. In Fig. 15 the predicted dependence of Φ_{p_T} on T fluctuations [34] is plotted and compared to Φ_{p_T} measured for the 5% most central Pb+Pb interactions. The experimental Φ_{p_T} value contains both short and long range correlations. The solid line corresponds to the T-fluctuation model presented in [34], which does not include short range correlations. The dashed line is the combination of this model with a contribution of short range correlations estimated experimentally [6] as 5 MeV/c, in agreement with theoretical arguments [13,14]. One sees that the observed value of Φ_{p_T} is already below the contribution of the Bose-Einstein correlations and that the inclusion of slope fluctuations makes the difference even larger. Thus, one can conclude, in agreement with the previous results [6], that the data leave no space for significant T fluctuations provided they are not canceled by other negative correlations.

An increase of transverse momentum fluctuations was predicted [18] to occur in A+A collisions which freeze-out

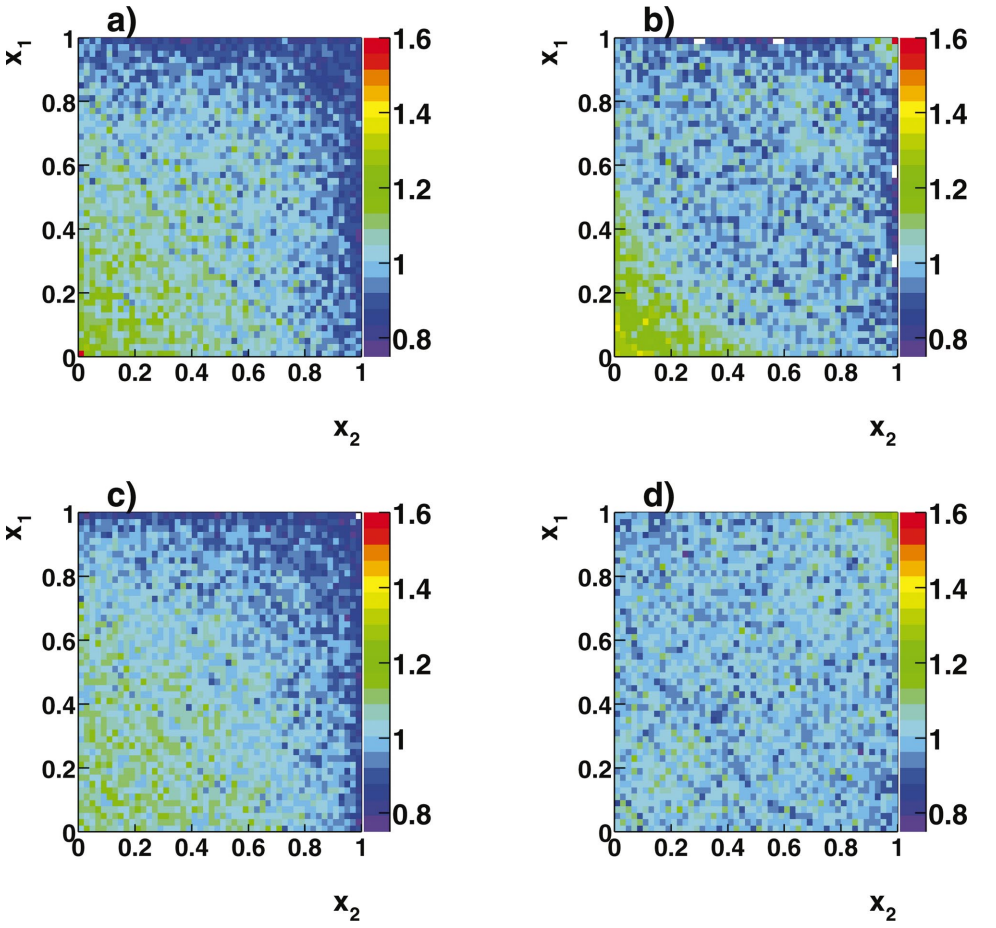

FIG. 12. (Color) Two-particle correlation plots using the cumulant p_T variable x. Results are shown for all charged particles for p+p data (a) compared to: simulated p+p HIJING events with limited NA49 acceptance (b), simple random-generator model, which reproduces $M(p_T)$ versus N correlation for p+p data (c), and model of fluctuations of the inverse slope parameter for p+p data on the level of about 10% (d).

near a second order critical end point of the QCD phase diagram. Based on calculations from [18] and the numbers given in Table III, it can be estimated that such critical fluctuations alone should result in $\Phi_{p_T} \simeq 20$ MeV/c. The limited acceptance is expected to reduce the signal to $\Phi_{p_T} \simeq 10$ MeV/c [46]. This number is comparable to the maximum value of Φ_{p_T} found in this analysis for peripheral Pb+Pb interactions ($\Phi_{p_T} = 7.2 \pm 0.7 \pm 1.6$ MeV). Note, however, that this theoretical estimate is subject to many uncertainties, among them how close the freeze-out is to the critical point. In order to learn whether the critical fluctuations are observed, measurements of Φ_{p_T} (as well as other fluctuation observables) as a function of energy are needed.

VII. SUMMARY

Transverse momentum event-by-event fluctuations were studied for p+p, C+C, Si+Si, and Pb+Pb collisions at 158 *A*GeV. The analysis was limited to the forward rapidity region. Three different characteristics were measured: the fluctuations of average transverse momentum $[M(p_T)]$ of the event, the Φ_{p_T} fluctuation measure, and transverse momentum two-particle correlations. All measured Φ_{p_T} values are below 10 MeV/c and are much smaller than the dispersion of the inclusive p_T distribution. However, the correlations observed in p+p collisions are not simply more and more diluted when going to heavier colliding systems, as could be expected if the created matter approaches a higher level of

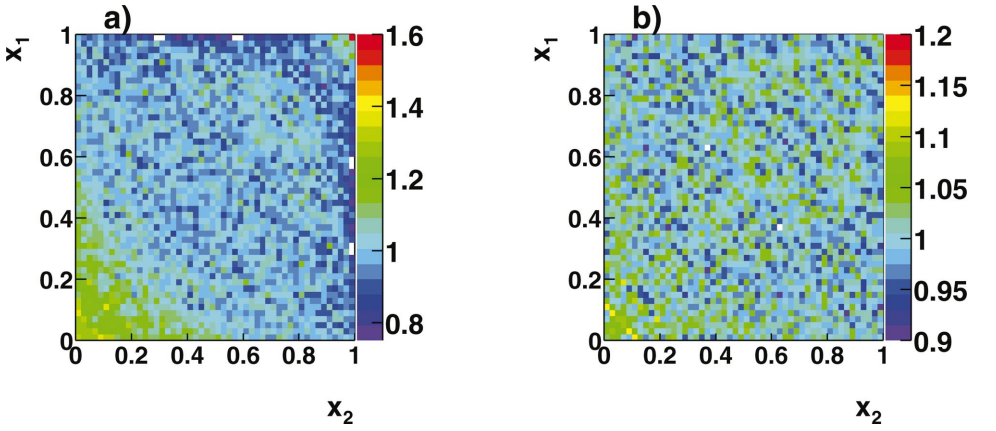

FIG. 13. (Color) Two-particle correlation plots using the cumulant p_T variable x. Results are shown for simulated p+p (a) and C+C (b) collisions from the HIJING model. Limited NA49 acceptance is taken into account.

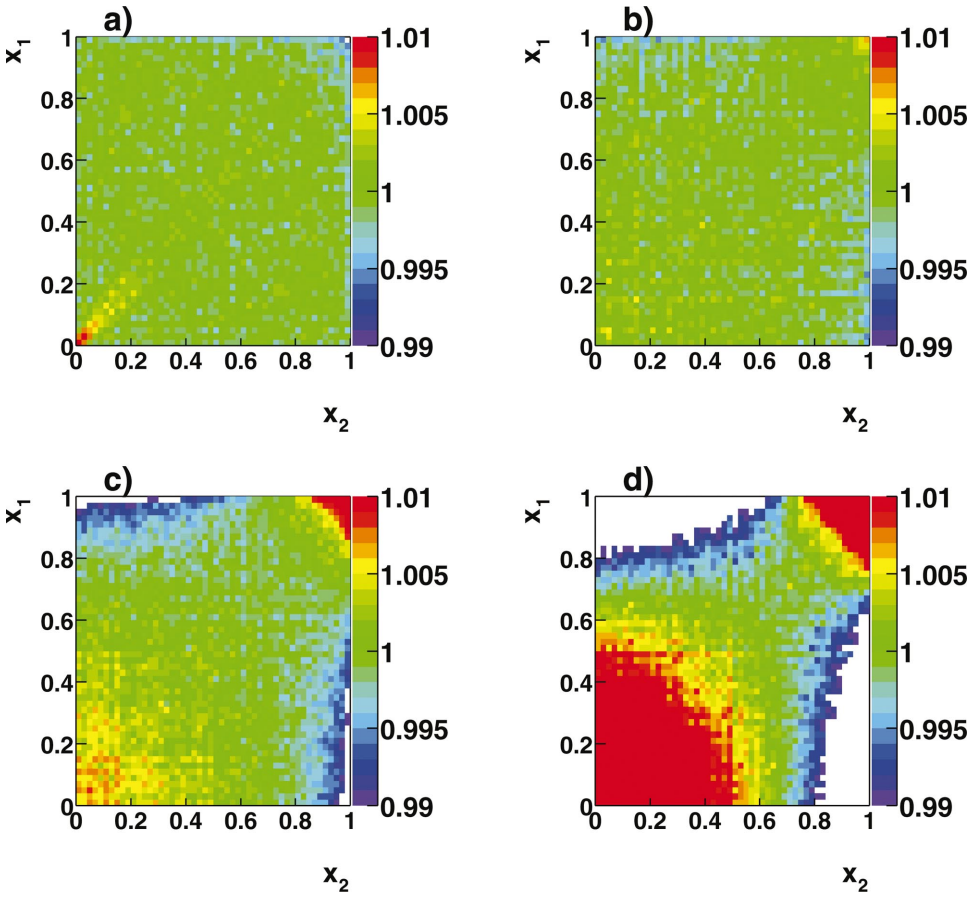

FIG. 14. (Color) Two-particle correlation plots using the cumulant p_T variable x for the most central Pb+Pb collisions. The experimental result is shown in (a) and compared to the inverse slope parameter fluctuation model (b)–(d). In the model the mean value of the inverse slope parameter was set to 190 MeV. The dispersions of the Gaussian shaped inverse slope parameter distributions were set to: σ_T=5 MeV (b), σ_T =10 MeV (c), and σ_T=20 MeV (d).

equilibrium with increasing system size. Instead, a significant system size dependence of the Φ_{p_T} measure is seen with a maximum for peripheral Pb+Pb collisions with $N_W \simeq 40$. The two-particle correlation plot for p+p data shows a prominent structure that was found to be connected with the dependence of $M(p_T)$ on N. This structure disappears when going to heavier colliding systems. Instead, short range correlations become visible as an enhancement of the point density in the region close to the diagonal. This effect is strongest for the most central Pb+Pb interactions. No structure characteristic of event-by-event temperature fluctuations is observed.

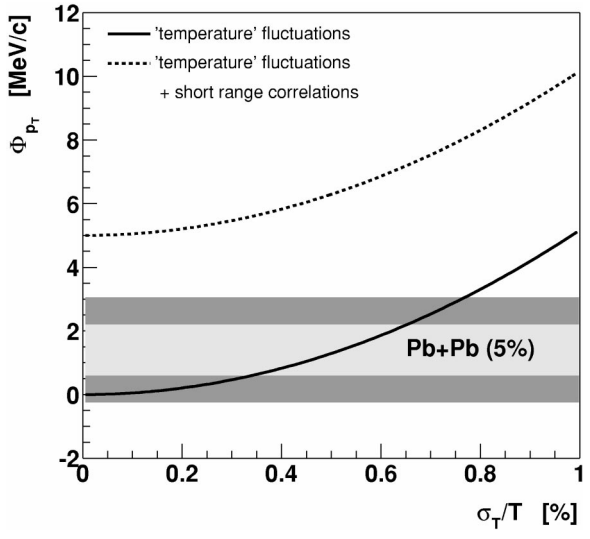

FIG. 15. Predicted dependence of Φ_{p_T} on T fluctuations [34] compared to the measured Φ_{p_T} for the 5% most central Pb+Pb collisions. The uncertainty of the measured Φ_{p_T} value is represented by the bands for statistical (gray) and systematic (dark gray) errors.

The HIJING model qualitatively reproduces the structure of two-particle correlation plots for p+p and C+C data. However, in contrast to the data, it shows no centrality dependence of Φ_{p_T}.

In future, a study of the energy dependence of transverse momentum fluctuations in the CERN SPS energy range is planned using the NA49 Pb+Pb collision data taken at different beam energies. The aim is to search for possible anomalies connected with the onset of the deconfinement phase transition, which is indicated by features of pion and strangeness production at low SPS energies [2,3].

ACKNOWLEDGMENTS

This work was supported by the Director, Office of Energy Research, Division of Nuclear Physics of the Office of High Energy and Nuclear Physics of the U.S. Department of Energy (DE-ACO3-76SFOOO98 and DE-FG02-91ER40609), the U.S. National Science Foundation, the Bundesministerium für Bildung und Forschung, Germany,

the Alexander von Humboldt Foundation, the U.K. Engineering and Physical Sciences Research Council, the Polish State Committee for Scientific Research (2 P03B 130 23, SPB/CERN/P-03/Dz 446/2002-2004, 2 P03B 02418, 2 P03B 04123, 2 P03B 023), the Hungarian Scientific Research Foundation (T032648, T14920, and T32293), Hungarian National Science Foundation, OTKA, (F034707), the EC Marie Curie Foundation, and the Polish-German Foundation.

[1] J. C. Collins and M. J. Perry, Phys. Rev. Lett. **34**, 1353 (1975); E. V. Shuryak, Phys. Rep. **61**, 71 (1980); **115**, 151 (1984).
[2] M. Gaździcki and M. I. Gorenstein, Acta Phys. Pol. B **30**, 2705 (1999).
[3] NA49 Collaboration, S. V. Afanasiev *et al.*, Phys. Rev. C **66**, 054902 (2002).
[4] For a review see: H. Heiselberg, Phys. Rep. **351**, 161 (2001).
[5] R. Stock, in *Proceedings of the NATO Advanced Study Workshop on Hot Hadronic Matter: Theory and Experiment*, Divonne-les-Bains, France, 1994.
[6] NA49 Collaboration, H. Appelshäuser *et al.*, Phys. Lett. B **459**, 679 (1999).
[7] S. V. Afanasiev *et al.*, Phys. Rev. Lett. **86**, 1965 (2001).
[8] NA22 Collaboration, M. R. Atayan *et al.*, Phys. Rev. Lett. **89**, 121802 (2002).
[9] CERES Collaboration, D. Adamova *et al.*, nucl-ex/0305002.
[10] STAR Collaboration, J. Adams *et al.*, nucl-ex/0308033.
[11] PHENIX Collaboration, J. Nystrand *et al.*, Nucl. Phys. A **A715**, 603 (2003).
[12] M. Gaździcki and St. Mrówczyński, Z. Phys. C **54**, 127 (1992).
[13] St. Mrówczyński, Phys. Lett. B **439**, 6 (1998).
[14] St. Mrówczyński, Phys. Lett. B **465**, 8 (1999).
[15] M. Gaździcki, Eur. Phys. J. C **8**, 131 (1999).
[16] St. Mrówczyński, Phys. Lett. B **459**, 13 (1999).
[17] L. Stodolsky, Phys. Rev. Lett. **75**, 1044 (1995); E. V. Shuryak, Phys. Lett. B **423**, 9 (1998).
[18] M. Stephanov, K. Rajagopal, and E. V. Shuryak, Phys. Rev. D **60**, 114028 (1999).
[19] St. Mrówczyński, Phys. Lett. B **430**, 9 (1998).
[20] E. V. Shuryak, Nucl. Phys. A **A715**, 289 (2003).
[21] G. Baym and H. Heiselberg, Phys. Lett. B **469**, 7 (1999).
[22] S. Jeon and V. Koch, Phys. Rev. Lett. **85**, 2076 (2000).
[23] M. Asakawa, U. Heinz, and B. Müller, Phys. Rev. Lett. **85**, 2072 (2000).
[24] N. G. Antoniou *et al.*, Phys. Lett. B **432**, 8 (1998).
[25] Z. Fodor and S. D. Katz, J. Hepatol **03**, 014 (2002).
[26] S. A. Voloshin *et al.*, Phys. Rev. C **60**, 024901 (1999).
[27] T. Trainor, hep-ph/0001148.
[28] STAR Collaboration R. L. Ray *et al.*, Nucl. Phys. A **715**, 45 (2003).
[29] M. Bleicher *et al.*, Phys. Lett. B **435**, 9 (1998).
[30] A. Capella, E. G. Ferreiro, and A. B. Kaidalov, hep-ph/9903338.
[31] F. Liu, A. Tai, M. Gaździcki, and R. Stock, Eur. Phys. J. C **8**, 649 (1999).
[32] O. V. Utyuzh, G. Wilk, and Z. Wlodarczyk, Phys. Rev. C **64**, 027901 (2001).
[33] R. Korus and St. Mrówczyński, Phys. Rev. C **64**, 054906 (2001).
[34] R. Korus, St. Mrówczyński, M. Rybczyński, and Z. Wlodarczyk, Phys. Rev. C **64**, 054908 (2001).
[35] NA49 Collaboration, J. G. Reid *et al.*, Nucl. Phys. **A661**, 407 (1999).
[36] A. Bialas and M. Gaździcki, Phys. Lett. B **252**, 483 (1990).
[37] NA49 Collaboration, L. S. Barnby *et al.*, J. Phys. G **25**, 469 (1999).
[38] NA49 Collaboration, S. Afanasiev *et al.*, Nucl. Instrum. Methods Phys. Res. A **430**, 210 (1999).
[39] K. Werner, Phys. Rep. **232**, 87 (1993).
[40] G. Cooper, Ph.D. thesis, University of California, Berkeley, 2000.
[41] C. Hoehne, Ph.D. thesis, Fachbereich Physik der Universität, Marburg, 2003.
[42] NA49 Collaboration, V. Friese *et al.* hep-ph/0111423 (2001).
[43] NA49 Collaboration, C. Alt *et al.*, Phys. Rev. C **68**, 034903 (2003).
[44] M. Gyulassy and X.-N. Wang, LBL-34246, 1997.
[45] A. I. Golokhvastov, JINR, P2-2003-52 (2003) (unpublished).
[46] M. A. Stephanov, Phys. Rev. D **65**, 096008 (2002), and private communication.